Annals of Physics **268**, 172–204 (1998)
Article No. PH985810

General Rydberg Atoms in Crossed Electric and Magnetic Fields: Calculation of Semiclassical Recurrence Spectra with Special Emphasis on Core Effects

Kirsten Weibert, Jörg Main, and Günter Wunner

Institut für Theoretische Physik I, Ruhr-Universität Bochum, D-44780 Bochum, Germany

Received December 22, 1997

The photoabsorption spectra of highly excited Rydberg atoms in external fields are known to be related to closed classical orbits of the excited electron. For atoms in a pure magnetic field, scaled recurrence spectra have successfully been calculated from classical orbits using the semiclassical closed-orbit theory. Rydberg atoms in crossed fields are more complicated as regards their theoretical and numerical treatment, as the Hamiltonian is nonseparable in three degrees of freedom, in contrast to only two nonseparable degrees of freedom in a pure magnetic field. In this paper, we present an extension of the closed-orbit theory to three degrees of freedom, taking into account arbitrary quantum defects. Motivated by nonhydrogenic resonances discovered in experimental scaled recurrence spectra of rubidium atoms, we investigate the influence of the ionic core on the three-dimensional closed orbits, using a simple model potential. We find that the introduction of a core potential results in an extreme increase of the number of closed orbits as compared to hydrogen. The novel orbits appear to be composed of hydrogenic orbits and are created through scattering by the core potential. Investigating the classical deflection function of the model potential, general properties of the new orbits can be explained. With the closed-orbit theory extended to three nonseparable degrees of freedom, we are able to calculate scaled recurrence spectra for Rydberg atoms in crossed fields with arbitrary quantum defects. Our results are in good agreement with the experimental spectra. In particular, the nonhydrogenic resonances can be explained in terms of the new orbits created by classical core scattering.

1. INTRODUCTION

Highly excited Rydberg atoms in magnetic fields as well as in crossed electric and magnetic fields have recently attracted much interest concerning the study of quantum chaos. These atoms represent quantum mechanical systems whose classical counterparts show chaotic behaviour. Due to the large spatial extension of the excited states, these systems are suited for a semiclassical approach, thus establishing a link between quantum mechanics and classical chaos [1–3]. Additionally, these atoms are also suited for experimental investigations [4–8], which makes them ideal objects for studying the quantum mechanical manifestations of classical chaos.

0003-4916/98 $25.00

The classically chaotic behaviour of these systems is a consequence of the fact that the corresponding Hamiltonian contains terms with different, incompatible symmetries, and therefore, is nonseparable.

In a pure magnetic field, the system still possesses a rotational symmetry about the direction of the magnetic field, so that the angular motion perpendicular to the magnetic field can be separated, which reduces the problem to a two-dimensional one. The remaining two-dimensional system is nonseparable. If the influence of the external field and the inner-atomic forces are comparably large, which is the case for highly excited atoms and usual laboratory field strengths, the system becomes highly nonintegrable, and classically behaves chaotic.

In crossed fields, the rotational symmetry is lost, and the Hamiltonian is nonseparable in three degrees of freedom. This renders the theoretical treatment more complicated, as now all calculations have to be performed in three dimensions instead of two. Up to now, theoretical investigations have mainly concentrated on Rydberg atoms in a pure magnetic field.

Historically, the first manifestations of classical chaos in quantum mechanical systems were found in 1969, when Garton and Tomkins discovered the quasi-Landau resonances, an oscillation of the absorption rate with energy, in barium atoms placed in a magnetic field [9]. In later experiments, many such oscillations were found for all kinds of Rydberg atoms in magnetic fields [4–6]. It turned out that the oscillations were connected to closed classical orbits of the excited electron. The contributions of the closed orbits are best visible in Fourier transformed spectra at constant scaled energy, where every orbit produces a sharp peak.

Du and Delos [10] and Bogomolny [11] presented a quantitative explanation of this phenomenon for hydrogen in a magnetic field following a semiclassical approach. Their closed-orbit theory connects the quantum mechanical absorption rate to classical closed orbits of the electron starting at and returning to the nucleus.

Later, the effects of an additional short-range core potential were investigated. Experimental spectra [6] and exact quantum defect R-matrix calculations [12, 13] of nonhydrogenic Rydberg atoms in a magnetic field showed oscillations that could not be explained in terms of hydrogenic closed orbits. It turned out that an additional core potential classically results in the creation of a huge number of new closed orbits, which appear to be composed of two or more hydrogenic orbits [14]. Their existence can be explained by the scattering of hydrogenic orbits by the core potential. Although the scattering takes place in a region where the semiclassical approximation is not valid, a rigorous semiclassical approach proved to be successful in explaining the new resonances [14]. Extending the closed-orbit theory to arbitrary quantum defects and including the nonhydrogenic core scattered orbits led to results which were in good agreement with experimental and quantum mechanical ones.

Recent experiments on Rydberg atoms in crossed electric and magnetic fields exhibited oscillations in the absorption spectra similar to those found in a pure magnetic field [7, 8]. A first understanding of the properties of the spectra

was achieved by considering planar hydrogenic orbits (running in the plane perpendicular to the magnetic field), which give the main contributions to the spectrum. However, no search for three-dimensional orbits was performed. Furthermore, the search for closed orbits was carried out only for the pure hydrogen potential, but the experimental spectra show resonances which have no counterparts in the hydrogen spectrum, which implies that core effects are important.

Our aim is to extend the closed-orbit theory to three nonseparable degrees of freedom and to investigate, as it was done for a pure magnetic field in [14], the effects of a short-range core potential on the absorption spectra in crossed fields. Because of the experimental results, we expect core scattering of hydrogenic orbits to have an important effect in crossed fields as well. As in [14], we undertake a rigorous semiclassical approach with classical treatment of the core effects.

Our paper is organized as follows: In Section 2, we give a brief description of the classical dynamics of the system, including the introduction of a model potential for the ionic core. We also perform a regularization of the equations of motion, which is important for numerical calculations. In Section 3, we present the novel types of orbits we found for general Rydberg atoms in crossed fields. Some properties of these orbits are explained with the help of the classical deflection function. In Section 4, we develop a modification of the closed-orbit theory for three nonseparable degrees of freedom and arbitrary quantum defects. Finally, in Section 5, we compare our results to the experimental rubidium spectra published in [8].

For convenience, all calculations are performed in atomic units.

2. CLASSICAL DYNAMICS

2.1. *Model Potential*

Our classical calculations start from the classical Hamiltonian of a general Rydberg atom in crossed fields. The full Hamiltonian contains all interactions between the nucleus, the electrons and the external fields. We are dealing with the excitation of Rydberg states, where only one electron is highly excited, while the ionic core remains in the ground state. We can therefore essentially simplify the problem by considering the Hamiltonian of a single electron moving in an effective potential produced by the nucleus and the other electrons and in crossed external fields. (The movement of the centre of mass of the system can be separated if the atom does not perform any motion perpendicular to the magnetic field.)

With the magnetic field pointing in the z- and the electric field pointing in the x-direction, the Hamiltonian of the excited electron reads

$$H = \tfrac{1}{2}\mathbf{p}^2 + \tfrac{1}{2}BL_z + \tfrac{1}{8}B^2\rho^2 + V(r) + Fx \tag{1}$$

(atomic units). Here, B and F are the magnetic and electric field strength, and $\rho = \sqrt{x^2 + y^2}$. $V(r)$ is the potential produced by the nucleus and the other electrons; we assume it to be spherically symmetric. The potential must obey the following asymptotic behaviour:

$$V(r) \xrightarrow{r \to 0} -\frac{Z}{r}, \qquad V(r) \xrightarrow{r \to \infty} -\frac{1}{r}, \tag{2}$$

where Z is the charge of the nucleus. As the core will usually be much smaller than the spatial extension of the excited state, the potential will differ from the purely hydrogenic potential only within a small region around the nucleus. We therefore write

$$V(r) = -\frac{1}{r} + V_{\text{core}}(r), \tag{3}$$

with a short-range core potential V_{core}.

With the spherically symmetric potential $V(r)$, the cylindrically symmetric diamagnetic part $\frac{1}{8}B^2\rho^2$, and the term Fx, the Hamiltonian contains contributions with three different, incompatible symmetries. This causes the problem to be nonseparable in three degrees of freedom. In the range of energy and field strengths of interest, the three terms with different symmetries are of the same order of magnitude, thus inducing chaotic behaviour of the system.

If we wished to describe a particular atom to high accuracy, we would have to choose $V(r)$ as realistic as possible. However, since we are mainly interested in qualitative effects, we use a simple model potential instead, which allows for an easy integration of the equations of motion. A suitable form was used for Rydberg atoms in a pure magnetic field by Hüpper *et al.* [14]:

$$V(r) = -\frac{1}{r}\left[1 + (Z-1)\, e^{-ar}(1 + ar)\right]. \tag{4}$$

The free parameter a is a measure for the extension of the core. Hüpper *et al.* proposed to choose a in such a way that the quantum defects of the atom in point are approximately reproduced. The reason was that the quantum defects are related to the classical deflection function, the latter playing an important role in the creation of new orbits through scattering by the core potential. For the reader's convenience, we briefly recapitulate the relation between deflection function and quantum defects:

The classical deflection function yields the scattering angle as a function of angular momentum for given energy $E > 0$:

$$\Theta(L) = \pi - \sqrt{2} \int_{r_0}^{\infty} \frac{L}{r^2 \sqrt{E - V(r) - (L^2/2r^2)}}\, dr. \tag{5}$$

Quantum mechanically, the short-range core potential causes phase shifts in the unbound states, which in semiclassical approximation can be calculated from the expression

$$\delta_l = \sqrt{2}\int_{r_0}^{\infty} \sqrt{E - V(r) - \frac{(l+\frac{1}{2})^2}{2r^2}}\, dr - \sqrt{2}\int_{r_{0,C}}^{\infty} \sqrt{E + \frac{1}{r} - \frac{(l+\frac{1}{2})^2}{2r^2}}\, dr. \tag{6}$$

At the field-free ionization threshold, $E = 0$, the phase shifts are connected to the quantum defects μ_l of the bound states by

$$\delta_l = \pi\mu_l. \tag{7}$$

From (5), (6), and (7) it can be found that for $E = 0$

$$\frac{d\mu_l}{dl} = \frac{1}{2\pi}\,\Theta(L)\Big|_{L=l+1/2}. \tag{8}$$

2.2. *Scaling Properties*

The hydrogenic Hamiltonian in crossed fields

$$H_H = \frac{1}{2}\,\mathbf{p}^2 + \frac{1}{2}\,BL_z + \frac{1}{8}\,B^2\rho^2 - \frac{1}{r} + Fx \tag{9}$$

possesses an important scaling property: If one defines the scaled quantities

$$\tilde{\mathbf{x}} = B^{2/3}\mathbf{x} \tag{10}$$

$$\tilde{\mathbf{p}} = B^{-1/3}\mathbf{p} \tag{11}$$

$$\tilde{H} = B^{-2/3}H; \qquad \tilde{E} = B^{-2/3}E \tag{12}$$

$$\tilde{F} = B^{-4/3}F \tag{13}$$

$$\tilde{t} = Bt \tag{14}$$

and for every quantity $G = f(\mathbf{x}, \mathbf{p}, t)$,

$$\tilde{G} = f(\tilde{\mathbf{x}}, \tilde{\mathbf{p}}, \tilde{t}), \tag{15}$$

the Hamiltonian $\tilde{H}$ and the resulting equations of motion

$$\frac{\partial \tilde{H}}{\partial \tilde{p}_i} = \frac{d\tilde{x}_i}{d\tilde{t}}, \qquad \frac{\partial \tilde{H}}{\partial \tilde{x}_i} = -\frac{d\tilde{p}_i}{d\tilde{t}} \qquad (i = 1, 2, 3) \tag{16}$$

become independent of B. In other words, the classical dynamics does not depend on all three parameters B, F, and E, but only on two parameters, $\tilde{E}$ and $\tilde{F}$. (This is in analogy to hydrogen in a pure magnetic field, where the dynamics is characterized by $\tilde{E}$ alone.)

With the additional core potential, the scaling property is no longer exact. The basic reason for this is that the extension of the core does not depend on the magnetic field strength. E.g., in the model potential (4), the parameter a determining the range of the core is a constant, and does not scale with B.

On the other hand, the range of the core potential is short compared to the extension of the excited state. Thus, apart from a small region around the nucleus, the Hamiltonian does still exhibit the above scaling properties. If the range of B considered is small enough, the classical dynamics can still be assumed to be independent of B. With the model potential (4), this is equivalent to assuming $B^{-2/3}a$ to be approximately constant. The classical dynamics, including the core potential, can then be calculated in scaled variables.

2.3. *Regularization of Equations of Motion*

The calculation of semiclassical recurrence spectra by means of closed-orbit theory requires the numerical search for closed orbits starting and ending exactly at the nucleus. This leads to numerical difficulties because of the singularity of the potential at the origin.

From the asymptotic behaviour of the potential for $r \to 0$ it can be seen that the singularity is a purely Coulombic one. A method for regularization of that type of singularity was presented by Kustaanheimo and Stiefel [15] (originally for the three-dimensional Kepler problem).

For Rydberg atoms in a pure magnetic field, the problem could be reduced to a two-dimensional one. The regularization could then be performed by introducing two semiparabolic coordinates and by transformation of the time [14]. As has been shown in [15], the regularization of the *three*-dimensional problem can only be achieved by transformation into a *four*-dimensional space.

We define (with a slight modification of the definition in [15]) four coordinates u_i by

$$\begin{aligned} x &= u_1 u_3 - u_2 u_4 \\ y &= u_1 u_4 + u_2 u_3 \\ z &= \tfrac{1}{2}(u_1^2 + u_2^2 - u_3^2 - u_4^2). \end{aligned} \tag{17}$$

The inverse transformation is not unique. The result is

$$\begin{aligned} u_1 &= \sqrt{r+z}\,\cos\frac{\varphi+\alpha}{2} \\ u_2 &= \sqrt{r+z}\,\sin\frac{\varphi+\alpha}{2} \\ u_3 &= \sqrt{r-z}\,\cos\frac{\varphi-\alpha}{2} \\ u_4 &= \sqrt{r-z}\,\sin\frac{\varphi-\alpha}{2}, \end{aligned} \tag{18}$$

where the angle α is arbitrary.

In order to ensure that the solutions found in the four-dimensional space satisfy the equations of motion in the three-dimensional Cartesian coordinates, the following additional condition has to be set up (cf. [15]):

$$u_1\dot{u}_2 - u_2\dot{u}_1 - u_3\dot{u}_4 + u_4\dot{u}_3 = 0. \tag{19}$$

The second step of the regularization consists in the introduction of the semi-parabolic time τ, defined by

$$d\tau = \frac{1}{\mathbf{u}^2}\,dt, \tag{20}$$

with $\mathbf{u}^2 = u_1^2 + u_2^2 + u_3^2 + u_4^2$. One then defines

$$K := \mathbf{u}^2 H(P_i, u_i) - \mathbf{u}^2 E, \tag{21}$$

where P_i are the conjugate momenta of u_i. It can easily be established that

$$\frac{\partial K}{\partial P_i} = \frac{du_i}{d\tau}, \qquad \frac{\partial K}{\partial u_i} = -\frac{dP_i}{d\tau}. \tag{22}$$

With the model potential (4), we obtain

$$\begin{aligned} K = {} & \tfrac{1}{2}\mathbf{P}^2 + \tfrac{1}{8}B^2\mathbf{u}^2(u_1^2+u_2^2)(u_3^2+u_4^2) \\ & + \tfrac{1}{2}B[(u_1^2+u_2^2)(u_3P_4 - u_4P_3) + (u_3^2+u_4^2)(u_1P_2 - u_2P_1)] \\ & - 2(1+(Z-1)\,e^{-(1/2)a\mathbf{u}^2}(1+\tfrac{1}{2}a\mathbf{u}^2)) \\ & + F\cdot\mathbf{u}^2(u_1u_3 - u_2u_4) - \mathbf{u}^2E. \end{aligned} \tag{23}$$

K and the resulting equations of motion (22) do not contain any singularity any more.

3. CREATION OF NEW CLOSED ORBITS THROUGH CLASSICAL CORE SCATTERING

3.1. *Numerical Search for Closed Orbits*

For the calculation of scaled recurrence spectra with the help of closed-orbit theory, all closed orbits up to a given scaled action have to be found. We give a short description of our search algorithm.

The three-dimensional orbits starting at the origin are characterized by the two starting angles θ_i and φ_i. For given energy and electric and magnetic field strength, we start trajectories from the origin into discrete starting directions separated by a stepwidth $(d\theta, d\varphi)$. For every starting direction, the equations of motion are integrated numerically in regularized coordinates using a predictor-corrector method with controlled order and stepwidth.

If during integration the distance r from the origin reaches a minimum, the integration is interrupted. We then try to optimize starting angles and time using a Newton procedure so that the trajectory returns to the nucleus as close as possible. Simultaneously, the parameters of the orbit—action, stability, and Maslov index—are computed. Afterwards, we continue the integration in order to find further minima of r. We stop the integration and pass over to the next starting direction when the action of the trajectory reaches a given maximum value.

The idea behind using a Newton procedure is that the position of the electron is uniquely determined by the starting angles and the time: $\mathbf{r} = \mathbf{r}(\theta_i, \varphi_i, t)$. A *closed* orbit is therefore characterized by $\mathbf{r}(\theta_i, \varphi_i, t_f) = 0$, where t_f is the recurrence time of the orbit.

For reasons explained in Section 4.3, we calculate the closed orbits with the core potential switched off at the start and before the final return to the nucleus. This switching off does not influence the shape of the orbits (because they start and return radially), but it does have an effect on the action and stability. The switching on and off takes place when the electron is in a region where it is not influenced by the core potential.

A problem of our search algorithm is that we cannot be sure to find *all* closed orbits up to a given action. Usually, very unstable orbits will not be found. The number of orbits found may sensitively depend on the stepwidth $(d\theta, d\varphi)$ chosen. On the other hand, it will be seen in Section 4.5 that very unstable orbits only contribute very little to the absorption spectrum. The error produced by leaving out the most unstable orbits will therefore usually be small.

Switching off the core potential in the beginning and in the end has the positive side effect that all closed orbits become more stable. This makes our search algorithm more effective.

3.2. *Types of Closed Orbits Found*

In this section, we present the types of closed orbits we found for general Rydberg atoms in crossed fields. As we were interested in demonstrating the qualitative

effects brought about by the nonhydrogenic structure of the atoms, we used the simple model potential (4) with a fixed value of the parameter a but different values of Z.

As we had expected on account of the results obtained for Rydberg atoms in a pure magnetic field [14], we observed that with increasing quantum defect (corresponding to increasing Z in our model potential) a huge number of new closed orbits is produced. As in the pure magnetic field, the new orbits appear to be composed of two or more hydrogenic orbits. (By hydrogenic orbits we mean orbits we find for the pure hydrogen potential.)

The orbits found can roughly be divided into two groups:

- hydrogen-like orbits,
- interconnections of hydrogen-like orbits.

The hydrogen-like orbits are identical with or similar to hydrogenic orbits. Hydrogenic orbits that do not come into the range of the core potential except at the start and at their final return can be found with exactly the same shape for general Rydberg atoms as well. As we switch off the core potential in the beginning and in the end, these orbits do not feel the core potential at all; their parameters (action, stability etc.) are exactly the same as for hydrogen. An example of such an orbit is shown in Fig. 1.

Hydrogenic orbits that do have intermediate contact with the core are disturbed by the core potential. Their shape is more or less distorted. Some of them undergo bifurcations and split into a set of similar orbits (see Fig. 2). Whereas the starting and returning angles, the action and the Maslov index remain similar to those of the original hydrogenic orbit, the stability may change drastically. (With the additional core potential the orbits are usually much less stable.) Many of the hydrogenic orbits disturbed by the core potential already look like interconnections of other hydrogenic orbits. Therefore we cannot draw a clear line between the two classes of orbits defined above.

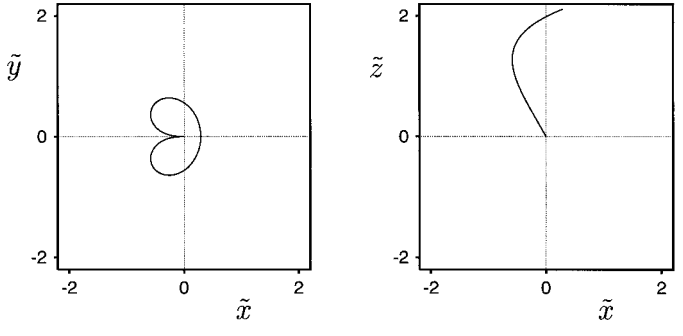

FIG. 1. Three-dimensional hydrogenic orbit which remains undisturbed by the core potential (plotted in scaled Cartesian coordinates), calculated at scaled energy $\tilde{E} = -0.3$ and scaled electric field strength $\tilde{F} = 0.1$.

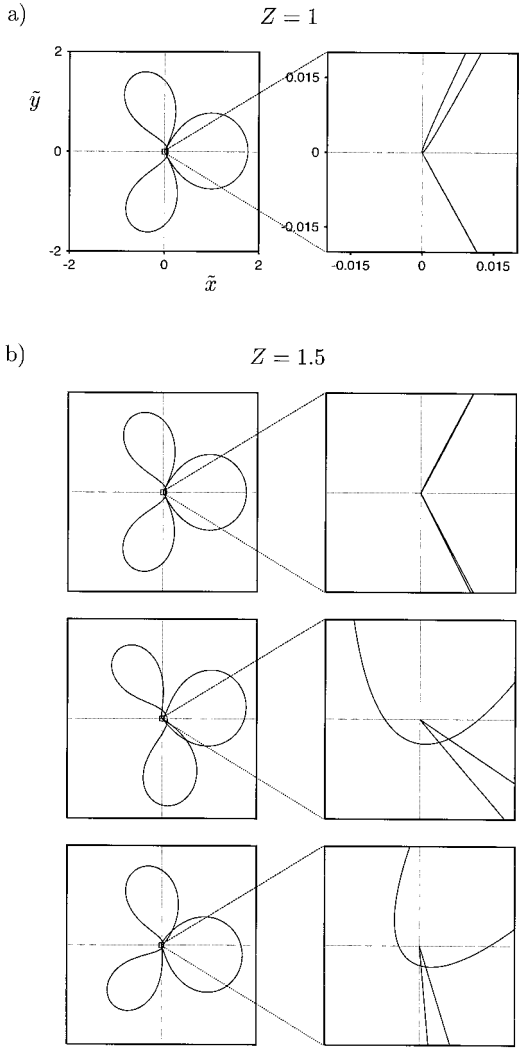

FIG. 2. Perturbation of a planar hydrogenic orbit by the core potential. The orbit undergoes a bifurcation and splits into three similar orbits. (a) Unperturbed hydrogenic orbit. (b) Perturbed orbits, determined for the model potential (4) with $Z = 1.5$ and $a = 1$. The scales in (b) are the same as in (a). The orbits were calculated at the parameters $\tilde{E} = -0.3$, $\tilde{F} = 0.1$ ($B = 2.5 \times 10^{-5}$ (a.u.)). For each orbit, a magnification of the core region is given.

Most of the orbits found belong to the group of interconnected hydrogenic orbits. The existence of these orbits can be explained by scattering of the electron by the core potential: The electron starts from the nucleus into a direction approximately equal to the starting direction of a hydrogenic orbit. It approximately follows the hydrogenic orbit, but, instead of exactly returning to the nucleus, it is deflected by the core potential. Accidentally, its outgoing direction

after scattering may approximately agree with the starting direction of another hydrogenic orbit. The electron then follows this orbit, and, when returning to the core, may be scattered again etc., until it finally returns exactly to the nucleus.

The action of such interconnected orbits is roughly, but not exactly, equal to the sum of the actions of their hydrogenic components. Their starting angles lie in the vicinity of the hydrogenic ones. The interconnected orbits are usually much less stable than their hydrogenic components, the stability falling rapidly with the number of components involved.

The interconnected orbits appear in families of orbits which have the same components but differ in the order in which the components are connected and in details of the scattering process. E. g., the electron can pass the nucleus on its left or on its right side, and for large quantum defects it can circle the nucleus a number of times before leaving the core again. For illustration, part of such a family is shown in Fig. 3.

3.3. *Classical Deflection Function*

Many of the observed effects of the core potential can be understood by the properties of the classical deflection function: The interconnection of two hydrogenic orbits is possible if the potential allows for a deflection angle connecting the returning direction of the first and the starting direction of the second orbit. This condition is not exact as the hydrogenic orbits are distorted when being connected, but it is a good approximation.

The deflection function gives the scattering angle as a function of angular momentum for an electron coming from and returning to infinite distance. In our case it is more reasonable to consider, instead, the deflection angle of the electron when running through the sphere in which the combined Coulomb and core potential dominate over the external fields, as it is this region where the interconnection of orbits takes place. (For the field strength values of interest here, this region has an extension of the order of 100 Bohr radii.) Figure 4 shows this deflection angle for our model potential with different values of Z at energy $E = 0$.

The main effect of regarding the deflection angle at finite instead of infinite distance is that for a purely hydrogenic potential the deflection angle is then not constantly π any more. This is more realistic: We observed hydrogenic orbits which themselves already appeared like interconnected hydrogenic orbits with deflection angles near to but not exactly equal to π.

It can be seen from the deflection function that for hydrogen only deflection angles smaller than π are possible. The deflection angle varies very slowly with angular momentum. This is the reason why we do not observe interconnections between all possible hydrogenic orbits for the pure hydrogen potential: The angular momenta necessary for connecting orbits with deflection angles substantially different from π are very large, thus leading to a very great distortion of the orbits involved. Either it is not possible to distort the orbits that much by variation of the starting angles, or the distorted components do not look similar to the original hydrogenic orbits any more. Of course, for large angular momentum, i. e. for large impact

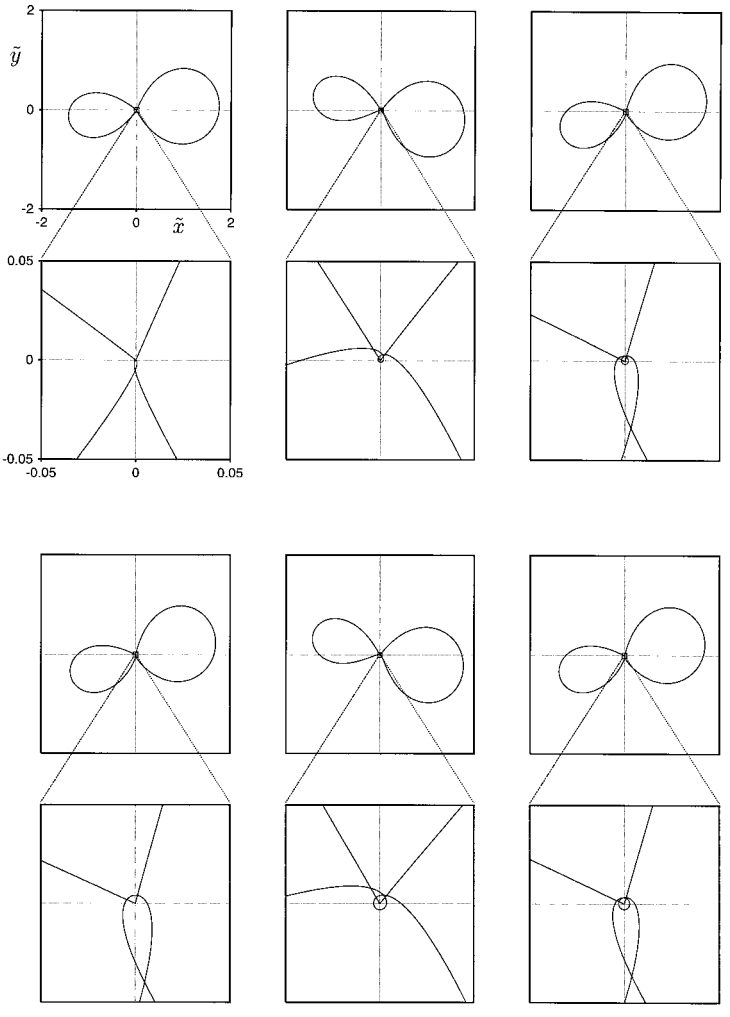

FIG. 3. Part of a family of interconnections between two planar hydrogenic orbits, found for the model potential (4) with $Z = 1.5$ and $a = 1$. The parameters are $\tilde{E} = -0.3$, $\tilde{F} = 0.1$ ($B = 2.5 \times 10^{-5}$ (a.u.)). All those members of the family are shown for which the electron runs through the left component of the orbit first. In each case a magnification of the core region is given. The scales are the same throughout the figure.

parameters, the influence of the external fields cannot be neglected any more. There is no way of distinguishing clearly between deflection by the Coulomb potential and deflection by the external fields. We therefore only speak of interconnected orbits when core effects are involved.

With growing Z, the deflection function exhibits a maximum value larger than π. For every deflection angle greater than π there are two possible values of the angular momentum. This is in agreement with the properties of the family of orbits

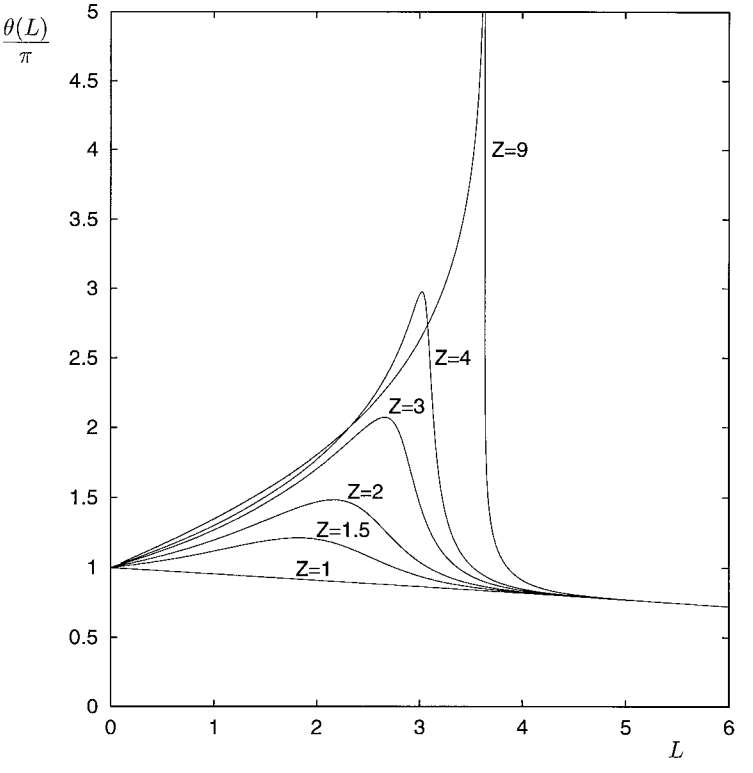

FIG. 4. Deflection angle $\theta(L)$ of the electron when running through a sphere of radius = 100 Bohr radii around the nucleus, as a function of angular momentum L, calculated for the model potential (4) with $a = 1$ and different values of Z.

shown in Fig. 3. The maximum deflection angle increases with growing quantum defect. This explains why the number of closed orbits increases with growing Z: For larger quantum defects, scattering angles greater than 2π are possible, which means that the electron can circle the nucleus once or several times before leaving the core region again. The greater the maximum deflection angle, the more numbers of circlings are possible, which implies that the number of possible ways of interconnecting two orbits increases.

For values of Z larger than about 5, the deflection function of our model potential exhibits a singularity (see Fig. 4): The maximum deflection angle becomes infinitely large, which means that the electron can be trapped by the core potential. The influence of such a singularity on semiclassical scattering cross sections was discussed by Berry and Mount [16]. In our case, the singularity leads to an infinite number of possible interconnections between two orbits given. On the other hand, the stability of the interconnected orbits usually decreases rapidly with the number of circlings during the scattering process (while the action increases by an

approximately constant amount with every circling). Therefore, even here, only a few orbits can contribute significantly to the absorption rate.

4. CLOSED-ORBIT THEORY FOR THREE NONSEPARABLE DEGREES OF FREEDOM AND ARBITRARY QUANTUM DEFECTS

In this section we present a modification of the closed-orbit theory for the case of a general Rydberg atom in crossed electric and magnetic fields. The closed-orbit theory was first developed for hydrogen in a magnetic field by Du and Delos [10] and by Bogomolny [11]. In [14] an extension to general Rydberg atoms in a magnetic field was presented. Whereas in a pure magnetic field the azimuthal φ motion in the plane perpendicular to the magnetic field can be separated, the problem of a Rydberg atom in crossed fields is nonseparable in three degrees of freedom. This requires a modification of the method, which we develop below. As in [14] we make a fully semiclassical approach with classical treatment of the core scattering.

4.1. *Basic Idea and Physical Picture*

Our calculation of semiclassical spectra follows the basic ideas presented by Du and Delos in [10]. For completeness, we briefly recapitulate the fundamental formulas and the physical picture.

As has been shown in [10], the absorption rate can be expressed in terms of the Green's function $G_E^+ = \lim_{\varepsilon \to 0} 1/(E - H + i\varepsilon)$,

$$\frac{dN}{dt} = -\frac{A}{\pi} \operatorname{Im} \langle \Psi_i D |\, G_E^+ \,| D\Psi_i \rangle \tag{24}$$

$$=: -\frac{A}{\pi} \operatorname{Im} \int (D\Psi_i)^* (\mathbf{x})\, F(\mathbf{x})\, d^3x, \tag{25}$$

where D is the projection of the dipole operator onto the direction of the polarization of the exciting laser beam, and A is a constant proportional to the number of atoms in the initial state and to the laser intensity.

The function $F(\mathbf{x}) = \langle \mathbf{x} |\, G_E^+ \,| D\Psi_i \rangle$ is a solution of the inhomogeneous Schrödinger equation

$$(E - H)\, F(\mathbf{x}) = (D\Psi_i)(\mathbf{x}). \tag{26}$$

The initial state $\Psi_i(\mathbf{x})$ and, as a consequence, $(D\Psi_i)(\mathbf{x})$ differ significantly from zero only in a small region (of a few Bohr radii) around the nucleus. Outside that region, $F(\mathbf{x})$ solves the Schrödinger equation for energy E. $F(\mathbf{x})$ can therefore be identified with a final state after excitation. The excited state will usually have an extension of a few thousand Bohr radii. Sufficiently far away from the nucleus, F can be approximated semiclassically. The calculation of the absorption rate only

requires the knowledge of F in the region near the nucleus, as only this region contributes to $\langle \Psi_i D | \, G_E^+ \, | D\Psi_i \rangle$.

Underlying our calculation of F in the relevant region is the following physical picture, which was first presented by Du and Delos in [10]: Initially, the electron is in a state located close to the nucleus. By excitation of the electron an outgoing wave F^{out} (satisfying (26)) is produced. Far away from the nucleus, where the problem can be treated semiclassically, parts of the wave follow classical trajectories. Some of these are finally turned back to the nucleus by the external fields, where they form a returning wave F^{ret}. The full wave is a superposition of the outgoing and the returning part,

$$F(\mathbf{x}) = F^{\text{out}}(\mathbf{x}) + F^{\text{ret}}(\mathbf{x}), \tag{27}$$

where F^{out} is a solution of (26) and F^{ret} solves the Schrödinger equation. Interference between incoming and outgoing waves leads to oscillations in the absorption rate.

Following this picture, our calculation of the absorption rate can be divided into the following steps: First, we have to find an expression for the outgoing wave F^{out} near the nucleus, where the nucleus and core potential dominate over the influence of the external fields. We then propagate this wave semiclassically into the region where the external fields become important, using the semiclassical approximation for nonintegrable systems developed by Maslov and Fedoriuk [17]. Finally, we calculate the returning quantum mechanical wave F^{ret} from those classical trajectories that return to the nucleus. In the semiclassical approximation, we also include the nonhydrogenic trajectories produced by intermediate core scattering.

In the case of a pure magnetic field, the magnetic quantum number m is conserved. Separating the φ dependence, every m channel can be treated separately, which reduces the problem to a two-dimensional one [10, 14]. In the case of crossed fields, m is not conserved and we have to propagate the three-dimensional wave as a whole. The semiclassical approximation will therefore involve three-dimensional trajectories with the amplitude of the semiclassical wave depending also on φ.

4.2. *Outgoing Wave*

In the vicinity of the core, the influence of the external fields can be neglected. Following the physical picture described above, the outgoing wave will be the same as if no external fields were present:

$$F^{\text{out}}(\mathbf{x}) = F^{\text{out}}_{\text{field-free}}(\mathbf{x}). \tag{28}$$

The outgoing wave F^{out} can therefore be calculated using the field-free Green's function $G^+_{E,\,\text{field-free}}$.

As we are interested only in highly excited states near the field-free ionization threshold, we can approximately set E equal to zero in the outgoing wave. The

field-free Green's function for $E=0$ is well known. In coordinate space we have [19]

$$\mathcal{G}^{+}_{E=0,\,\text{field-free}}(\mathbf{x},\mathbf{x}')=\sum_{l,m} Y^{*}_{lm}(\theta',\varphi')\; g^{0}_{l}(r,r')\; Y_{lm}(\theta,\varphi), \tag{29}$$

with

$$g^{0}_{l}(r,r')=\frac{2R^{0,\,\text{reg}}_{l}(r_{<})\,R^{0,\,\text{out}}_{l}(r_{>})}{r'^{2}\mathcal{W}(R^{0,\,\text{reg}}_{l}(r'),\,R^{0,\,\text{out}}_{l}(r'))}. \tag{30}$$

In (30), $\mathcal{W}$ is the Wronskian, and

$$r_{<}=\min(r,r')$$
$$r_{>}=\max(r,r').$$

The functions $R^{0,\,\text{reg}}_{l}$ and $R^{0,\,\text{out}}_{l}=R^{0,\,\text{reg}}_{l}+iR^{0,\,\text{irreg}}_{l}$ are the regular and the outgoing solutions of the radial part of Schrödinger's equation for $E=0$. Outside the range of the core potential, the regular and the irregular solution can be written as superpositions of Bessel and Neumann functions,

$$R^{0,\,\text{reg}}_{l}(r)=\frac{1}{\sqrt{8r}}\left(\cos\delta_{l}J_{2l+1}(\sqrt{8r})-\sin\delta_{l}N_{2l+1}(\sqrt{8r})\right) \tag{31}$$

$$R^{0,\,\text{irreg}}_{l}(r)=\frac{1}{\sqrt{8r}}\left(\cos\delta_{l}N_{2l+1}(\sqrt{8r})+\sin\delta_{l}J_{2l+1}(\sqrt{8r})\right) \tag{32}$$

$$R^{0,\,\text{out}}_{l}(r)=\frac{1}{\sqrt{8r}}\,e^{i\delta_{l}}\left(J_{2l+1}(\sqrt{8r})+iN_{2l+1}(\sqrt{8r})\right), \tag{33}$$

with the asymptotic forms

$$R^{0,\,\text{reg}}_{l}(r)\to\left(\frac{2}{\pi\sqrt{8r}}\right)^{1/2}\frac{1}{\sqrt{8r}}\cos\left(\sqrt{8r}-\left(l+\frac{1}{2}\right)\pi-\frac{\pi}{4}+\delta_{l}\right) \tag{34}$$

$$R^{0,\,\text{irreg}}_{l}(r)\to\left(\frac{2}{\pi\sqrt{8r}}\right)^{1/2}\frac{1}{\sqrt{8r}}\sin\left(\sqrt{8r}-\left(l+\frac{1}{2}\right)\pi-\frac{\pi}{4}+\delta_{l}\right) \tag{35}$$

$$R^{0,\,\text{out}}_{l}(r)\to\left(\frac{2}{\pi\sqrt{8r}}\right)^{1/2}\frac{1}{\sqrt{8r}}\exp\left[\,i\left(\sqrt{8r}-\left(l+\frac{1}{2}\right)\pi-\frac{\pi}{4}+\delta_{l}\right)\right] \tag{36}$$

for large r. The phase shifts δ_{l} depend on the explicit form of the core potential.

The Wronskian can be shown to be

$$\mathcal{W}(R^{0,\,\text{reg}}_{l}(r'),\,R^{0,\,\text{out}}_{l}(r'))=\frac{i}{8\pi r'^{2}}. \tag{37}$$

Outside the core region, we now obtain the following expression for the outgoing wave:

$$F^{\text{out}}(\mathbf{x}) = \int \mathcal{G}^{+}_{E=0,\,\text{field-free}}(\mathbf{x}, \mathbf{x}')(D\Psi_i)(\mathbf{x}')\, d^3x'$$

$$= -16\pi i \sum_{l,m} R_l^{0,\,\text{out}}(r)\, Y_{lm}(\theta, \varphi) \underbrace{\int R_l^{0,\,\text{reg}}(r')\, Y_{lm}^*(\theta', \varphi')(D\Psi_i)(\mathbf{x}')\, d^3x'}_{=:\, B_{lm}}. \quad (38)$$

The coefficients B_{lm} cannot be calculated analytically for nonhydrogenic atoms because this would require the knowledge of an analytic form of the initial wave function Ψ_i. On the other hand, as the external fields can be neglected in the region near the nucleus, Ψ_i can be expanded into spherical harmonics:

$$\Psi_i(\mathbf{x}) = \sum_{l',m'} b_{l'm'} R_{nl'}(r)\, Y_{l'm'}(\theta, \varphi) \quad (39)$$

for fixed quantum number n. For low-lying initial states, the sum includes only few values of l'. The action of the dipole operator upon the initial state is

$$(D\Psi_i)(\mathbf{x}) = r(a^+ \sin\theta\, e^{i\varphi} + a^- \sin\theta\, e^{-i\varphi} + a^0 \cos\theta)\, \Psi_i(\mathbf{x}), \quad (40)$$

with a^+, a^-, and a^0 determining the direction of polarization.

Using the above relations, the integral B_{lm} reads

$$B_{lm} = \sum_{l',m'} b_{l'm'} \int R_l^{0,\,\text{reg}}(r)\, r R_{nl'}(r)\, r^2\, dr$$

$$\times \int Y_{lm}^*(\theta, \varphi)(a^+ \sin\theta\, e^{i\varphi} + a^- \sin\theta\, e^{-i\varphi} + a^0 \cos\theta)\, Y_{l'm'}(\theta, \varphi) \sin\theta\, d\theta\, d\varphi. \quad (41)$$

The angular integrals in (41) can be evaluated explicitly. As the sum includes only a few values of l', it follows that B_{lm} will be different from zero only for few values of l, m. The radial integrals, which are independent of m, cannot be calculated analytically for nonhydrogenic atoms.

We will compare our results to experimental spectra of rubidium atoms published in [8]. In this experiment, the initial state was the 5S ground state of rubidium. The polarization of the laser was along the external electric field, i.e. in the x-direction. For this case we have $\Psi_i(\mathbf{x}) = R_{50}(r)\, Y_{00}(\theta, \varphi)$, and $a^+ = a^- = \frac{1}{2}$, $a^0 = 0$. The only nonvanishing quantities B_{lm} in this case are B_{11} and B_{1-1} with $B_{11} = -B_{1-1}$.

4.3. *Semiclassical Propagation*

The outgoing wave F^{out} can now be propagated semiclassically into the region where the external fields become important. We use the semiclassical approximation for nonintegrable systems developed by Maslov and Fedoriuk [17]:

A solution of Schrödinger's equation correct in first order of h is constructed from classical trajectories started on an initial surface. In our case it is convenient to choose as the initial surface the surface of a sphere around the nucleus from which the trajectories have to be started radially outwards. The radius r_i of this sphere has to be chosen in such a way that the following conditions hold:

(a) $(D\Psi_i)(\mathbf{x}) \approx 0$,

(b) the potential can be approximated by its asymptotic form $-1/r$,

(c) the external fields can still be neglected compared to the Coulomb potential,

(d) the semiclassical approximation is valid.

For the field strengths of interest these conditions hold for r_i of the order of 100 Bohr radii.

Points on the initial sphere can be described by a pair of parameters (ω_1, ω_2), e.g. by the spherical polar coordinates (θ, φ). The latter have the disadvantage of not being isotropic. We introduce locally isotropic coordinates (ω_1, ω_2) both corresponding to arc lengths on great circles on the sphere. Our coordinates are defined by the following relations for every point $\mathbf{x}_i = (x_i, y_i, z_i)$ on the initial sphere (radius r_i):

$$\frac{\partial \mathbf{x}_i}{\partial \omega_1} = r_i \begin{pmatrix} \cos\theta \cos\varphi \\ \cos\theta \sin\varphi \\ -\sin\theta \end{pmatrix}, \qquad \frac{\partial \mathbf{x}_i}{\partial \omega_2} = r_i \begin{pmatrix} -\sin\varphi \\ \cos\varphi \\ 0 \end{pmatrix}, \tag{42}$$

where (θ, φ) is the direction of $\mathbf{x}_i$ in spherical polar coordinates.

To the semiclassical wave function at a given point $\mathbf{x}$ all those trajectories contribute that start at the initial surface and pass through $\mathbf{x}$. The contributions are of the form

$$\psi(\mathbf{x}) = A(\mathbf{x})\, e^{i(S(\mathbf{x}) - (\pi/2)\mu)}, \tag{43}$$

with

$$S(\mathbf{x}) = \int_{\mathbf{x}_0}^{\mathbf{x}} \mathbf{p} \cdot d\mathbf{x} + S_0 \tag{44}$$

the classical action integrated along the trajectory and

$$A(\mathbf{x}) = A_0 \sqrt{|J(t_i, \omega_1, \omega_2)\, J^{-1}(t, \omega_1, \omega_2)|}. \tag{45}$$

Here,

$$J(t, \omega_1, \omega_2) = \det\left(\frac{\partial \mathbf{x}}{\partial(t, \omega_1, \omega_2)}\right) \tag{46}$$

is the Jacobian determinant with ω_1 and ω_2 the starting parameters of the trajectory on the sphere. In (45), t_i is the time when the trajectories are started, and t is the time when the trajectory reaches $\mathbf{x}$. The Maslov index μ counts the singular points along the trajectory, i. e., points where the Jacobian determinant vanishes. These are the points where the semiclassical approximation breaks down [17, 18].

The constants A_0 and S_0 have to be chosen in such a way that the semiclassical wave is joined correctly to the exact quantum mechanical solution. They are obtained from the quantum mechanical solution on the initial sphere. The semiclassically propagated wave then reads

$$F_{\text{semi}}(\mathbf{x}) = \sum_k \sqrt{|J_k(t_i, \omega_1^{(k)}, \omega_2^{(k)})\, J_k^{-1}(t_k, \omega_1^{(k)}, \omega_2^{(k)})|}\; e^{i(S_k(\mathbf{x}) - (\pi/2)\mu_k)} F^{\text{out}}(\mathbf{x}_i^{(k)}). \tag{47}$$

The sum includes all classical trajectories with energy E started radially on the initial sphere and passing through $\mathbf{x}$. In (47), $\mathbf{x}_i^{(k)}$ is the starting point of the kth orbit on the initial sphere.

For points $\mathbf{x}$ close to, but outside the initial surface, F_{semi} contains, on the one hand, trajectories coming directly from the initial surface without ever leaving the vicinity of the nucleus, and, on the other hand, trajectories that have traveled away from the nucleus and have been turned back by the external fields. The latter form the semiclassical approximation of the returning part of F.

The returning wave F^{ret} itself consists of contributions from two different kinds of trajectories: The first kind passes through a given point $\mathbf{x}$ when coming in from the region outside the vicinity of the nucleus (incoming trajectories), the other kind first travels around the ionic core and passes through $\mathbf{x}$ when leaving the core again (outgoing trajectories).

It can be shown that each incoming trajectory passing through a given point $\mathbf{x}$ lies in the vicinity of a trajectory running exactly through the nucleus. As all trajectories are started radially on the initial sphere and the external fields can be neglected in this region, the trajectories can also, formally, be started at the nucleus. The incoming contributions to F^{ret} can therefore approximately be calculated from closed orbits starting and ending exactly at the nucleus.

The relations between the incoming trajectories contributing to F^{ret} and the closed orbits can be expressed in a closed analytical form if we calculate the closed orbits with the core potential switched off in the beginning and before their final return to the nucleus. Let $S_0^{(k)}$ and $\mu_0^{(k)}$ be the action and Maslov index of such a closed orbit. Using the parameterization defined by (42), the following relations can be established for the corresponding incoming contribution to F^{ret} (for the derivation of these relations see Appendix A):

$$|J_k(t_i, \omega_1^{(k)}, \omega_2^{(k)})| = \sqrt{2} r_i^{3/2} \tag{48}$$

$$|J_k(t_k, \omega_1^{(k)}, \omega_2^{(k)})| = 2\sqrt{r(1+\cos\gamma_k)}\,|M_0^{(k)}| \tag{49}$$

$$\mu_k = \mu_0^{(k)} - 1 \tag{50}$$

$$S_k = S_0^{(k)} - \sqrt{8 r_i} - 2\sqrt{r(1+\cos\gamma_k)}. \tag{51}$$

Here, r_i is the radius of the initial sphere, $r = |\mathbf{x}|$, and γ_k is the angle between $\mathbf{x}$ and the direction $(\theta_f^{(k)}, \varphi_f^{(k)})$ from which the closed orbit returns to the nucleus.

$M_0^{(k)}$ is related to the stability matrix of the closed orbit. For a closed orbit returning to the nucleus exactly from the z-direction $(\theta_f^{(k)} = 0)$ it is given by

$$M_0 = \left[\frac{1}{2r} \det \begin{pmatrix} \dfrac{\partial x}{\partial \omega_1} & \dfrac{\partial x}{\partial \omega_2} \\ \dfrac{\partial y}{\partial \omega_1} & \dfrac{\partial y}{\partial \omega_2} \end{pmatrix} \right]_{\mathbf{x}=0}. \tag{52}$$

The general case $(\theta_f^{(k)} \neq 0)$ is obtained from this by rotation.

Inserting (48)–(51) for the incoming parts in (47), we obtain the semiclassical approximation for F^{ret}:

$$F_{\mathrm{semi}}^{\mathrm{ret}}(\mathbf{x}) = \sum_k \left(2^{-1/4} i\, r_i^{3/4} \frac{e^{i(S_0^{(k)} - (\pi/2)\mu_0^{(k)})}}{\sqrt{|M_0^{(k)}|}} \cdot \frac{\exp[-2i\sqrt{r(1+\cos\gamma_k)}]}{[r(1+\cos\gamma_k)]^{1/4}} \times e^{-i\sqrt{8 r_i}} F^{\mathrm{out}}(\mathbf{x}_i^{(k)}) + F_k^{\mathrm{scat,out}}(\mathbf{x}) \right). \tag{53}$$

The sum now contains all closed orbits starting at and returning exactly to the nucleus. The closed orbits have to be calculated with the core potential switched off in the beginning and before the final return to the nucleus. The term $F_k^{\mathrm{scat,out}}(\mathbf{x})$ represents the contributions from trajectories passing through $\mathbf{x}$ when going out again.

Equation (53) can be expanded in terms of spherical harmonics using:

$$\frac{\exp[-2i\sqrt{r(1+\cos\gamma_k)}]}{[r(1+\cos\gamma_k)]^{1/4}} = 8\pi^{3/2} \sum_{l,m} (-1)^l\, Y_{lm}^*(\theta_f^{(k)}, \varphi_f^{(k)}) Y_{lm}(\theta, \varphi) \frac{1}{\sqrt{8r}} \left(\frac{2}{\pi\sqrt{8r}} \right)^{1/2} \times \exp\left(-i \left[\sqrt{8r} - \left(l + \frac{1}{2} \right) \pi \right] \right). \tag{54}$$

(We establish this expansion in Appendix B.) Here, $\theta_f^{(k)}$ and $\varphi_f^{(k)}$ are the returning angles of the closed orbit.

Inserting (54) and (38) into (53) and replacing $R_l^{0,\,\mathrm{out}}$ with its asymptotic form (36) we finally obtain

$$\begin{aligned} F_{\mathrm{semi}}^{\mathrm{ret}}(\mathbf{x}) = \sum_k \Bigg(& -32\pi^2 \frac{e^{i(S_0^{(k)} - (\pi/2)\mu_0^{(k)})}}{\sqrt{|M_0^{(k)}|}} \cdot \sum_{l',\,m'} (-1)^{l'}\, e^{i\delta_{l'}} B_{l'm'}\, Y_{l'm'}(\theta_i^{(k)},\, \varphi_i^{(k)}) \\ & \times \sum_{l,\,m} (-1)^l\, Y_{lm}^*(\theta_f^{(k)},\, \varphi_f^{(k)})\, Y_{lm}(\theta,\, \varphi)\, \frac{1}{\sqrt{8r}} \left(\frac{2}{\pi\sqrt{8r}} \right)^{1/2} \\ & \times \exp\left(-i \left[\sqrt{8r} - \left(l + \frac{1}{2} \right) \pi - \frac{\pi}{4} \right] \right) + F_k^{\mathrm{scat,\,out}}(\mathbf{x}) \Bigg) \\ =: & \sum_k F_{\mathrm{semi},\,k}^{\mathrm{ret}}(\mathbf{x}). \end{aligned} \tag{55}$$

Here, $\theta_i^{(k)}$ and $\varphi_i^{(k)}$ are the starting angles of the kth closed orbit. The above result is independent of the radius of the initial sphere.

4.4. *Returning Waves*

The semiclassical expression (55) is valid only sufficiently far away from the nucleus. We now have to find the exact quantum solution in the vicinity of the nucleus. As discussed in Section 4.1, F^{ret} is a solution of Schrödinger's equation in that region. We assume that every contribution F_k^{ret} is a stationary scattering wave as it would be produced by a plane-wave source at infinite distance. These scattering waves can be expanded in terms of the regular solutions of the radial part of Schrödinger's equation and spherical harmonics. As in the outgoing wave, from which we started, we set $E = 0$ and neglect the external fields:

$$F_k^{\mathrm{ret}}(\mathbf{x}) = \sum_{l,\,m} A_{lm} R_l^{0,\,\mathrm{reg}}(r)\, Y_{lm}(\theta,\, \varphi). \tag{56}$$

For sufficiently large r, we can use the asymptotic form (34) of $R_l^{0,\,\mathrm{reg}}$ so that

$$F_k^{\mathrm{ret}}(\mathbf{x}) = \frac{1}{\sqrt{8r}} \left(\frac{2}{\pi\sqrt{8r}} \right)^{1/2} \sum_{l,\,m} A_{lm}\, Y_{lm}(\theta,\, \varphi) \cos\left(\sqrt{8r} - \left(l + \frac{1}{2} \right) \pi - \frac{\pi}{4} + \delta_l \right). \tag{57}$$

By splitting the cosine in (57) into incoming and outgoing parts, $\cos x = \frac{1}{2}(e^{ix} + e^{-ix})$, and comparing the incoming parts of (55) and (57), the coefficients A_{lm} of the expansion can be determined. This leads to the following final result for the returning wave:

$$\begin{aligned} F^{\mathrm{ret}}(\mathbf{x}) = & -64\pi^2 \sum_k \frac{e^{i(S_0^{(k)} - (\pi/2)\,\mu_0^{(k)})}}{\sqrt{|M_0^{(k)}|}} \cdot \sum_{l',\,m'} (-1)^{l'}\, e^{i\delta_{l'}} B_{l',\,m'}\, Y_{l'm'}(\theta_i^{(k)},\, \varphi_i^{(k)}) \\ & \times \sum_{l,\,m} (-1)^l\, Y_{lm}^*(\theta_f^{(k)},\, \varphi_f^{(k)})\, e^{i\delta_l} R_l^{0,\,\mathrm{reg}}(r)\, Y_{lm}(\theta,\, \varphi). \end{aligned} \tag{58}$$

This expansion of F^{ret} is valid in the whole region in which the external fields can be neglected.

4.5. *Fourier Transformed Spectra at Constant Scaled Energy and Electric Field*

With the above results we can finally calculate the absorption rate:

$$\frac{dN}{dt} = -\frac{A}{\pi}\,\mathrm{Im}\int (D\Psi_i)^*(\mathbf{x})\,F^{\text{out}}(\mathbf{x})\,d^3x - \frac{A}{\pi}\,\mathrm{Im}\int (D\Psi_i)^*(\mathbf{x})\,F^{\text{ret}}(\mathbf{x})\,d^3x \tag{59}$$

$$=: \left.\frac{dN}{dt}\right|^{0} + \left.\frac{dN}{dt}\right|^{\text{osc}}. \tag{60}$$

The first part $(dN/dt)|^0$ containing the outgoing wave forms a continuous, slowly varying background of the spectrum. The second part, which is composed of contributions from the returning closed orbits, leads to oscillations in the spectrum, as we will see below. Inserting F^{ret} from (58), we obtain for the second part

$$\left.\frac{dN}{dt}\right|^{\text{osc}} = A\cdot 64\pi\,\mathrm{Im}\sum_k \left(\frac{e^{i(S_0^{(k)} - (\pi/2)\mu_0^{(k)})}}{\sqrt{|M_0^{(k)}|}} \sum_{l',m'} (-1)^{l'} e^{i\delta_{l'}} B_{l',m'}\, Y_{l'm'}(\theta_i^{(k)}, \varphi_i^{(k)}) \right.$$

$$\left. \times \sum_{l,m} (-1)^{l} e^{i\delta_l} B_{lm}^{*}\, Y_{lm}^{*}(\theta_f^{(k)}, \varphi_f^{(k)}) \right). \tag{61}$$

For excitation from an s state and polarization in the x-direction we had found $B_{11} = -B_{1-1}$, and all other B_{lm} vanish (cf. Section 4.2). As we cannot calculate B_{11} analytically, we leave it as an unknown constant factor. Inserting the above relations for the B_{lm} into (61) yields

$$\left.\frac{dN}{dt}\right|^{\text{osc}} \sim \sum_k \frac{\sin\theta_i^{(k)} \sin\theta_f^{(k)} \cos\varphi_i^{(k)} \cos\varphi_f^{(k)}}{\sqrt{|M_0^{(k)}|}} \sin\left(S_0^{(k)} - \frac{\pi}{2}\mu_0^{(k)} + 2\delta_1 \right). \tag{62}$$

Each contribution to (62) shows a sinusoidal dependence on the action of the corresponding closed orbit. For the latter we obtain by Taylor expansion around a given energy E_0:

$$S \approx S|_{E=E_0} + \left.\frac{dS}{dE}\right|_{E=E_0} \cdot (E - E_0)$$

$$= S|_{E=E_0} + T|_{E=E_0} \cdot (E - E_0), \tag{63}$$

where T denotes the classical recurrence time of the orbit [10]. That means every closed orbit causes a sinusoidal oscillation with energy in the absorption rate. A Fourier transformation of the absorption rate should produce peaks at the corresponding times T_k. However, the energy dependence of the other quantities in (62) is too strong for sharp peaks to appear.

The visibility of the peaks can be improved essentially by performing spectroscopy at constant scaled energy and electric field, as was done in the experiment described in [8]. In the experiment, the electric and magnetic field strength are varied synchronously with energy in such a way that the scaled energy $\tilde{E} = B^{-2/3}E$ and scaled electric field strength $\tilde{F} = B^{-4/3}F$ remain constant.

Expressed in terms of the scaled quantities

$$\tilde{S}_0^{(k)} = B^{1/3} S_0^{(k)} \tag{64}$$

$$\tilde{M}_0^{(k)} = B^{2/3} M_0^{(k)} \tag{65}$$

(cf. (15)), the oscillatory part of the absorption rate reads

$$\left.\frac{dN}{dt}\right|^{\text{osc}} \sim \frac{1}{\beta} \sum_k \frac{\sin\theta_i^{(k)} \sin\theta_f^{(k)} \cos\varphi_i^{(k)} \cos\varphi_f^{(k)}}{\sqrt{|\tilde{M}_0^{(k)}|}} \sin\left(\beta\tilde{S}_0^{(k)} - \frac{\pi}{2}\mu_0^{(k)} + 2\delta_1\right), \tag{66}$$

with the definition $\beta := B^{-1/3}$.

The experiment can only cover a finite range $[\beta_1, \beta_2]$ of β. If this range is small enough, $1/\beta$ will not vary much with β compared to the sine term. Due to the scaling properties of the Hamiltonian the other quantities depend only weakly on β if the scaled energy and the scaled electric field are kept constant. They can be approximated by their values obtained for a mean value of β. Fourier transforming (66) with respect to β will therefore lead to distinct peaks at the scaled actions $\tilde{S}_0^{(k)}$ of the closed orbits involved.

Approximating $1/\beta$ by $1/\bar{\beta}$ and assuming the scaled quantities to be independent of β, we obtain the following result for the Fourier transform of (66):

$$F(S) \sim \frac{1}{\bar{\beta}} \sum_k \frac{\sin\theta_i^{(k)} \sin\theta_f^{(k)} \cos\varphi_i^{(k)} \cos\varphi_f^{(k)}}{\sqrt{|\tilde{M}_0^{(k)}|}} \cdot \frac{\sin\left(\Delta\beta(\tilde{S}_0^{(k)} - S)\right)}{(\tilde{S}_0^{(k)} - S)}$$
$$\times i \exp\left[-i(\bar{\beta}\tilde{S}_0^{(k)} - \frac{\pi}{2}\mu_0^{(k)} + 2\delta_1)\right] \cdot e^{i\bar{\beta}S}, \tag{67}$$

with the definitions

$$\begin{aligned} \bar{\beta} &:= \tfrac{1}{2}(\beta_1 + \beta_2) \\ \Delta\beta &:= \tfrac{1}{2}(\beta_2 - \beta_1). \end{aligned} \tag{68}$$

In order to obtain a real quantity and to get rid of the strongly oscillating factor $e^{i\bar{\beta}S}$, it is convenient to multiply (67) by its complex conjugate. This yields

$$|F(S)|^2 \sim \left[\sum_k A_k^2 \left(\frac{\sin(\Delta\beta(\tilde{S}_0^{(k)} - S))}{(\tilde{S}_0^{(k)} - S)} \right)^2 + 2 \sum_{i<j} A_i A_j \frac{\sin(\Delta\beta(\tilde{S}_0^{(i)} - S))}{(\tilde{S}_0^{(i)} - S)} \frac{\sin(\Delta\beta(\tilde{S}_0^{(j)} - S))}{(\tilde{S}_0^{(j)} - S)} \times \cos\left(\bar{\beta}(\tilde{S}_0^{(i)} - \tilde{S}_0^{(j)}) - \frac{\pi}{2}(\mu_0^{(i)} - \mu_0^{(j)}) \right) \right], \tag{69}$$

with

$$A_k := \frac{\sin\theta_i^{(k)} \sin\theta_f^{(k)} \cos\varphi_i^{(k)} \cos\varphi_f^{(k)}}{\sqrt{|\tilde{M}_0^{(k)}|}}. \tag{70}$$

(It is the quantity $|F(S)|^2$ which is plotted in the experimental spectra published in [8].) The closed orbits from which $|F(S)|^2$ is obtained are to be calculated at a mean value of β.

In (69), every closed orbit produces a peak of the form $\sin^2(\Delta\beta(\tilde{S}_0^{(k)} - S))/(\tilde{S}_0^{(k)} - S)^2$, with its maximum at the scaled action $S_0^{(k)}$ of the orbit. The width of the peaks depends on the range over which the Fourier transformation is performed. The second sum in (69) contains interference terms between orbits with similar actions.

It is remarkable that (69) does not depend explicitly on the phase shifts δ_l caused by the core potential. The core potential influences (69) only through the creation of new closed orbits. This is due to the ground state and direction of polarization we chose, and therefore must be considered as a coincidence.

5. COMPARISON WITH EXPERIMENT

Experimental Fourier transformed spectra at constant scaled energy and electric field strength of rubidium Rydberg atoms in crossed fields were published by Raithel *et al.* in [8]. A description of the experimental setup can be found in [7, 8].

We compare these experimental spectra with the corresponding semiclassical spectra we calculated using the closed-orbits theory described in Section 4. For our calculations concerning rubidium we employed a model potential slightly different from (4), which was proposed in [20]:

$$V(r) = -\frac{1}{r}[1 + (Z-1)e^{-a_1 r} + a_2 r e^{-a_3 r}]. \tag{71}$$

The idea is that by having three free parameters instead of one the model potential can be fitted more accurately to the quantum defects of rubidium (cf. Section 2.1). Suitable values of the three parameters are [21]:

$$a_1 = 3.425$$
$$a_2 = 10.09 \tag{72}$$
$$a_3 = 1.595.$$

The classical deflection function of this model potential possesses a singularity, as was the case for the simple potential (4) with large values of Z (cf. Section 3.3). This turns out to have much more influence on the creation of new orbits through core scattering than the exact fitting of the parameters to the quantum defects. The actual choice of the parameters is therefore not really important.

Figure 5 shows some of the experimental spectra published in [8]. The quantity plotted corresponds to the quantity $|F(S)|^2$ defined in Section 4.5 (apart from a constant factor).

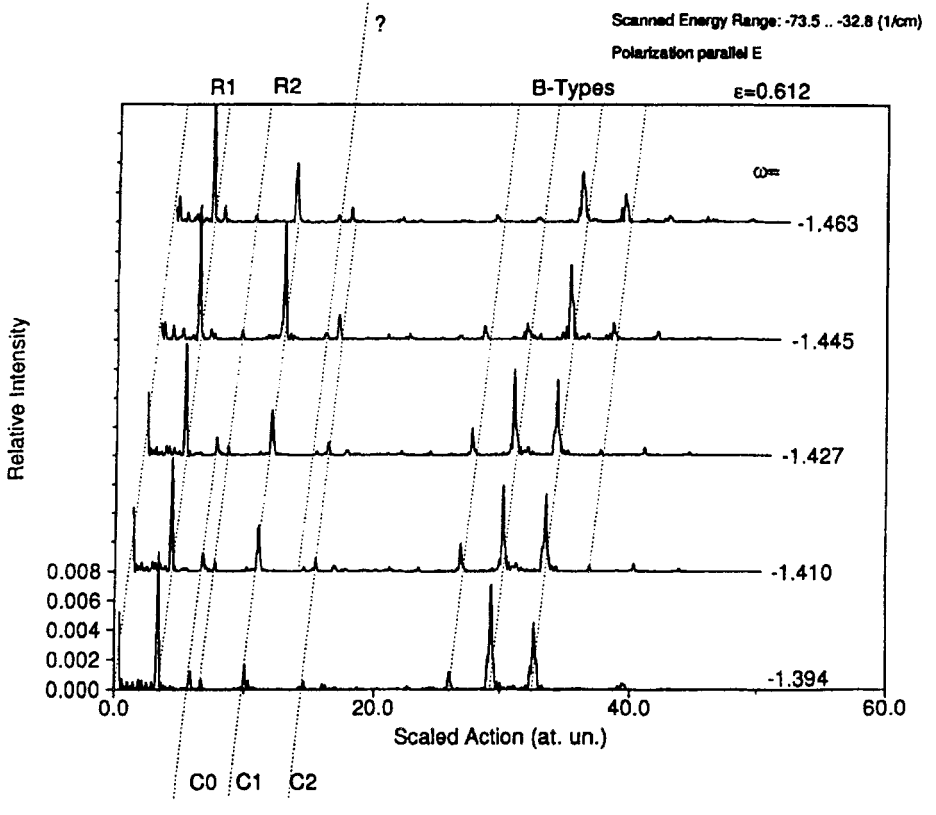

FIG. 5. Experimental scaled recurrence spectra of rubidium Rydberg atoms reproduced from [8] with kind permission of the authors and of the publisher, IOP Publishing Ltd. The spectra were taken at scaled electric field strength $\tilde{F}(=\varepsilon) = 0.612$ and different values of the scaled energy $\tilde{E}(=\omega)$.

Figure 6 shows the semiclassical spectrum calculated for the parameters $\tilde{E} = -1.427$, $\tilde{F} = 0.612$ ($B = 1.84 \times 10^{-6}$ (a.u.)) by means of closed-orbit theory with the model potential given above. For comparison, we also calculated the same spectrum with the pure hydrogenic potential.

The peaks labeled R and C in the semiclassical rubidium spectrum are caused by planar hydrogenic orbits (running in the x-y-plane). Figure 7 shows the orbits belonging to the R1 and the C1 peak. At the scaled action of the small peak labeled with a question mark, no hydrogenic orbit exists. This peak is caused by a large family of nonhydrogenic orbits, namely interconnections between the R1 and the C1 orbits. (Some examples are given in Fig. 8.) At a scaled action of about 33, another peak caused by interconnected orbits can be seen which does not have any counterpart in the semiclassical hydrogen spectrum. In fact, we find new closed

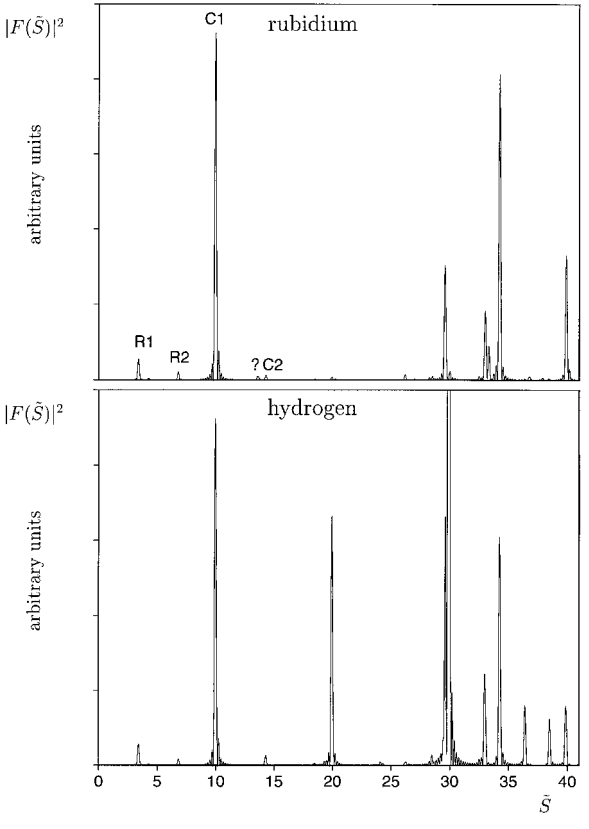

FIG. 6. Semiclassical recurrence spectra of rubidium and hydrogen, calculated for the parameters $\tilde{E} = -1.427$, $\tilde{F} = 0.612$ ($B = 1.84 \cdot 10^{-6}$ (a. u.)). For rubidium, the model potential (71) with the parameter values (72) was used. The large peak at $\tilde{S} \approx 30$ in the hydrogen spectrum is about five times larger than the range of $|F(\tilde{S})|^2$ shown. (This value, however, is unphysical: The parameters lie near a bifurcation point of the corresponding orbits, where the semiclassical approximation breaks down.)

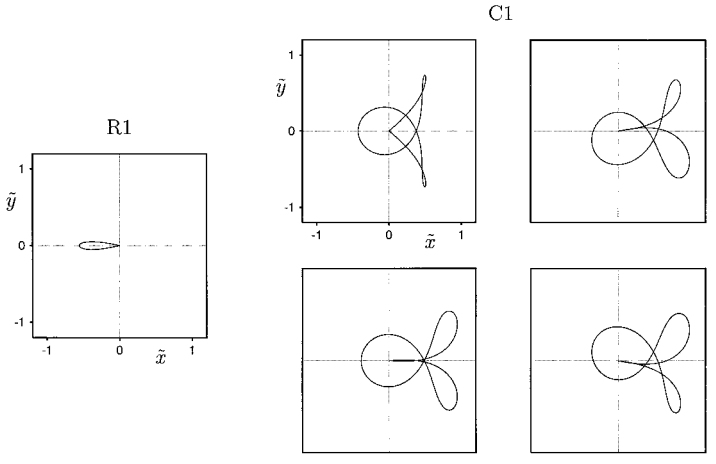

FIG. 7. The orbits causing the R1 and the C1 peak in the experimental spectra shown in Fig. 5 (all planar), calculated for the parameters $\tilde{E} = -1.427$, $\tilde{F} = 0.612$. The scaled actions of the four C1 orbits differ by less then 3×10^{-2}.

orbits at many scaled actions where no corresponding hydrogenic orbits exist. But except for the two peaks mentioned, all interconnected orbits are so unstable that they do not produce visible peaks.

Apart from the appearance of additional peaks, the semiclassical rubidium and hydrogen spectrum differ in the height of the hydrogenic peaks. Here, the two effects of the additional core potential—creation of new closed orbits and distortion of hydrogenic orbits—can be seen.

Concerning the position of the peaks, the experimental and the semiclassical rubidium spectrum are in quite good agreement. However, the peak labeled C0 in the experimental spectrum, and a second peak with a scaled action of about 15, are missing in the semiclassical spectrum. We only find the corresponding closed orbits if we use slightly different values of the scaled energy and electric field strength. We suppose that either the experimental parameters given in [8] were slightly incorrect or that these peaks are caused by complex ghost orbits [22]. This question must be left for future investigations.

The relative heights of the peaks do not always agree with the experimental ones. This is certainly partly due to the simple model potential we used. Whereas the positions of the peaks, i. e. the scaled actions of the interconnected orbits, should be nearly independent of the model potential, the stability of the interconnected orbits determining the height of the peaks sensitively depends on the potential used. In order to reproduce the heights of the peaks, we therefore would have to use a much more realistic core potential. Nevertheless, it should be noted that the relative heights of the peaks in the semiclassical rubidium spectrum are in better agreement with the experimental results than those calculated with the pure hydrogen potential.

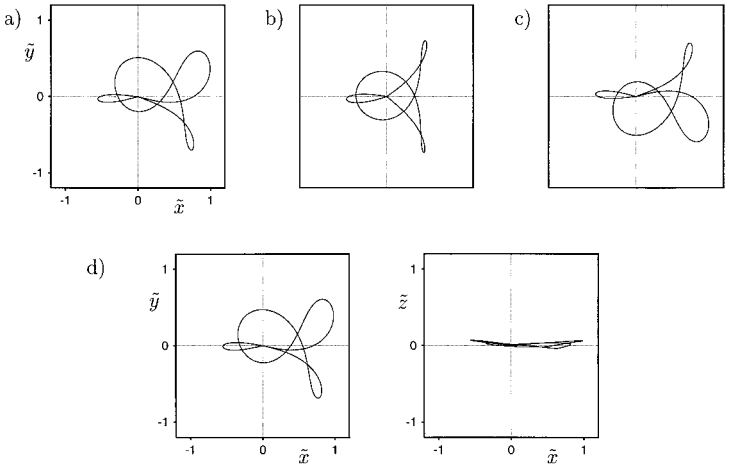

FIG. 8. Some examples of interconnections between the R1 and the C1 orbits at $\tilde{E} = -1.427$, $\tilde{F} = 0.612$ ($B = 1.84 \times 10^{-6}$ (a.u.)), found for the model potential (71) with the parameter values (72). The orbits (a)–(c) are planar, (d) is slightly out of the plane.

Clearly, the semiclassical spectrum with additional core potential reproduces the experimental spectrum much better than the semiclassical hydrogen spectrum.

6. CONCLUSION

We have investigated highly excited Rydberg atoms in crossed electric and magnetic fields. These atoms represent a system nonseparable in three degrees of freedom which behaves classically chaotic.

For classical calculations we have taken into account the effect of the core electrons by adding a simple short-range core potential to the hydrogen potential. We then investigated the influence of this core potential on the existence of closed classical orbits starting at and returning to the nucleus. We found that the main effect of the core potential, apart from disturbing hydrogenic orbits, is the creation of a huge number of new closed orbits. These new orbits appear to be composed of two or more hydrogenic orbits and originate from the scattering of hydrogenic orbits by the core potential.

By a modification of the closed-orbit theory for three nonseparable degrees of freedom and arbitrary quantum defects, we determined a semiclassical formula for the absorption spectra of Rydberg atoms in crossed fields. We followed a rigorous semiclassical approach with classical treatment of the core scattering.

Our results are in good qualitative agreement with experimental spectra. In particular, nonhydrogenic resonances in the experimental spectra can be explained with the new orbits created by core scattering. In order to also reproduce the

heights of the peaks in the Fourier transformed spectra, it will be necessary to use a more realistic model potential.

APPENDIX A: RELATIONS BETWEEN RETURNING TRAJECTORIES AND EXACTLY CLOSED ORBITS

A.1. *Jacobian Determinant on the Initial Sphere*

The Jacobian determinant of the outgoing trajectories on the initial sphere is given by (46) with $t = t_i$. As the trajectories start radially from the sphere, the time derivatives are given by

$$\begin{aligned} \dot{x} &= \dot{r} \sin\theta \cos\varphi \\ \dot{y} &= \dot{r} \sin\theta \sin\varphi \\ \dot{z} &= \dot{r} \cos\theta. \end{aligned} \tag{73}$$

Inserting (73) and the derivatives (42) into (46) yields after a short calculation

$$J_i = (r^2 \dot{r})|_{r=r_i}. \tag{74}$$

In the vicinity of the nucleus, the external fields can be neglected. For radial trajectories ($L = 0$), the Hamiltonian with the core potential switched off then reads

$$H = \frac{1}{2}\dot{r}^2 - \frac{1}{r} = E. \tag{75}$$

From the approximation $E = 0$ it follows that $\dot{r} = \sqrt{2/r}$, so that

$$J(t_i, \omega_1, \omega_2) = \sqrt{2}\, r_i^{3/2}. \tag{76}$$

A.2. *Jacobian Determinant of the Returning Trajectories*

Let us consider a trajectory returning approximately from the z-direction. Sufficiently far away from the nucleus, $\dot{x}$ and $\dot{y}$ can be neglected compared to $\dot{z}$, hence

$$J(t_k, \omega_1, \omega_2) \approx \dot{z} \cdot \det \begin{pmatrix} \dfrac{\partial x}{\partial \omega_1} & \dfrac{\partial x}{\partial \omega_2} \\ \dfrac{\partial y}{\partial \omega_1} & \dfrac{\partial y}{\partial \omega_2} \end{pmatrix}. \tag{77}$$

As $E \approx 0$, in the vicinity, but outside, the range of the core, the returning orbit approximately follows the branch of a parabola. Assuming that the corresponding

closed orbit returns exactly from the z-direction, the parabola is symmetric about the z-axis and can be described by the equation

$$r(\theta) = \frac{L^2}{1 - \cos\theta}, \tag{78}$$

where

$$L = r^2\dot{\theta} = \text{const} \tag{79}$$

is the angular momentum. Using (78) and (79), it can be established that

$$\dot{z} = \dot{r} = -\sqrt{(1 + \cos\theta)/r}. \tag{80}$$

Introducing a factor $2r$ for convenience, we therefore obtain

$$|J(t_k, \omega_1, \omega_2)| = 2\sqrt{r(1 + \cos\theta)}\,|M(\mathbf{x})|, \tag{81}$$

with

$$M(\mathbf{x}) = \frac{1}{2r}\det\begin{pmatrix} \dfrac{\partial x}{\partial \omega_1} & \dfrac{\partial x}{\partial \omega_2} \\ \dfrac{\partial y}{\partial \omega_1} & \dfrac{\partial y}{\partial \omega_2} \end{pmatrix}. \tag{82}$$

$M(\mathbf{x})$ is nearly constant in the vicinity of the nucleus if we switch off the core potential. We can therefore replace it with its value M_0 obtained for the exactly closed orbit at its final return to the nucleus.

The above result is valid only if the closed orbit returns along the z-axis. The general result can be obtained by rotation, replacing θ with the angle between $\mathbf{x}$ and the direction from which the closed orbit returns, and replacing $M(\mathbf{x})$ with the corresponding rotated matrix.

A.3. *Classical Action of the Returning Trajectory*

The trajectories used for the semiclassical approximation produce a momentum field $\mathbf{p}(\mathbf{x})$ which is not necessarily unique but can be divided into different branches. The trajectories have to be chosen in such a way that if we restrict ourselves to one branch, the classical action integral is locally path independent [17]. Instead of integrating along the nearly closed trajectory running through $\mathbf{x}$ (formally started at the origin), we can therefore integrate along the corresponding closed orbit (starting and ending at the origin), and then from the origin radially outwards to $\mathbf{x}$ (see Fig. 9).

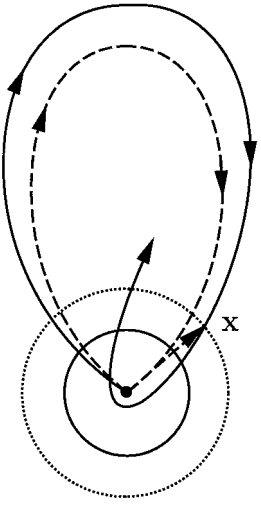

FIG. 9. Calculation of the action of the incoming orbits contributing to the semiclassical approximation: Instead of integrating from the origin to **x** along the nearly closed orbit (solid line), one can integrate along the corresponding closed orbit and then from the origin radially outwards to **x** (dashed line).

If we switch off the core potential in the end, the returning trajectories lying in the vicinity of the closed orbit follow parabolas. Assuming that the closed orbit returns from the z-direction, the parabolas can be described by (78). From (78) it follows that the radial part of the momentum field is given by

$$p_r = \dot{r} = -\sqrt{(1+\cos\theta)/r}. \tag{83}$$

Integrating radially from the origin to **x** therefore yields

$$\Delta S = \int_0^r p_r \, dr = -2\sqrt{r(1+\cos\theta)}. \tag{84}$$

If the closed orbit returns from an arbitrary direction, θ has to be replaced with the angle γ between **x** and the returning direction.

The trajectories contributing to the semiclassical approximation have to be started on the initial sphere. By starting them in the origin instead, we have an additional contribution S_i to the action. From (75) for radially outgoing trajectories with the core potential switched off, it followed that $\dot{r} \approx \sqrt{2/r}$, so that

$$S_i = \int_0^{r_i} \dot{r} \, dr = \sqrt{8 r_i}. \tag{85}$$

We therefore obtain for the action of the returning trajectory (started on the initial sphere and ending in $\mathbf{x}$),

$$S = S_0 - S_i + \Delta S = S_0 - \sqrt{8r_i} - 2\sqrt{r(1+\cos\gamma)}, \tag{86}$$

where S_0 is the action of the closed orbit.

A.4. *The Maslov Index of the Returning Orbit*

The Maslov index of a trajectory increases by one when the trajectory passes through the origin. The closed orbit must therefore have a Maslov index which is by one larger than the Maslov index of the returning orbit.

Strictly speaking, the Maslov index of the closed orbit formally has to be increased by $\frac{1}{2}$ at the start and at the final return the nucleus. This can be found from the form of the quantum mechanically correct outgoing and incoming solutions in the vicinity of the nucleus (see the phase $-\pi/4$ if we insert the asymptotic form (36) into our expression (38) for the outgoing wave).

APPENDIX B: EXPANSION OF THE SEMICLASSICAL RETURNING WAVE IN TERMS OF SPHERICAL HARMONICS

Here, we give a proof of the expansion (54). It is well known, that for $|x| \gg \nu$ the Bessel functions have the asymptotic form

$$J_\nu(x) = \sqrt{\frac{2}{\pi x}} \cos\left(x - \frac{\nu\pi}{2} - \frac{\pi}{4}\right). \tag{87}$$

Taking $\nu = 0$ and substituting $x = 2\sqrt{r(1+\cos\gamma)}$ leads to

$$\frac{\cos(2\sqrt{r(1+\cos\gamma)} - (\pi/4))}{[r(1+\cos\gamma)]^{1/4}} = \sqrt{\pi}\, J_0(2\sqrt{r(1+\cos\gamma)}) \tag{88}$$

for sufficiently large r. On the other hand, it was shown in [10], that

$$J_0(2\sqrt{r(1+\cos\gamma)}) = \sum_l \frac{2l+1}{\sqrt{2}} (-1)^l P_l(\cos\gamma) \frac{J_{2l+1}(\sqrt{8r})}{\sqrt{r}} \tag{89}$$

Here, γ is the angle between the direction (θ, φ) of $\mathbf{x}$ and the direction (θ_f, φ_f) from which the closed orbit returns. The well-known expansion of P_l into spherical harmonics therefore reads

$$P_l(\cos\gamma) = \frac{4\pi}{2l+1} \sum_m Y^*_{lm}(\theta_f, \varphi_f)\, Y_{lm}(\theta, \varphi). \tag{90}$$

Inserting (90) and the asymptotic form (87) of the Bessel function into (89) leads to the expansion

$$\frac{\cos[2\sqrt{r(1+\cos\gamma)}-(\pi/4)]}{[r(1+\cos\gamma)]^{1/4}} = 8\pi^{3/2}\sum_{l,m}(-1)^l\, Y^*_{lm}(\theta_f^{(k)},\varphi_f^{(k)})\, Y_{lm}(\theta,\varphi)\,\frac{1}{\sqrt{8r}}\left(\frac{2}{\pi\sqrt{8r}}\right)^{1/2} \times\cos\left(\sqrt{8r}-\left(l+\frac{1}{2}\right)\pi-\frac{\pi}{4}\right) \tag{91}$$

Splitting both cosines in (91) into incoming and outgoing parts, $\cos x=\frac{1}{2}(e^{ix}+e^{-ix})$, and comparing the incoming parts on both sides of (91) leads to (54).

REFERENCES

1. H. Friedrich and D. Wintgen, *Phys. Rep.* **183** (1989), 37.
2. H. Hasegawa, M. Robnik, and G. Wunner, *Prog. Theor. Phys.* **98** (1989), 198.
3. S. Watanabe, *in* "Review of Fundamental Processes and Applications of Atoms and Ions" (C. D. Lin, Ed.), World Scientific, Singapore, 1993.
4. A. Holle, G. Wiebusch, J. Main, B. Hager, H. Rottke, and K. H. Welge, *Phys. Rev. Lett.* **56** (1986), 2594. J. Main, G. Wiebusch, A. Holle, and K. H. Welge, *Phys. Rev. Lett.* **57** (1987), 2789.
5. T. van der Veldt, W. Vassen, and W. Hogervorst, *Europhys. Lett.* **21** (1993), 903.
6. D. Delande, K. T. Taylor, M. H. Halley, T. van der Veldt, W. Vassen, and W. Hogervorst, *J. Phys. B* **27** (1994), 2771.
7. G. Raithel, M. Fauth, and H. Walther, *Phys. Rev. A* **44** (1991), 1898.
8. G. Raithel, H. Held, L. Marmet, and H. Walther, *J. Phys. B* **27** (1994), 2849.
9. W. R. S. Garton and F. S. Tomkins, *Astrophys. J.* **158** (1969), 839.
10. M. L. Du and J. B. Delos, *Phys. Rev. A* **38** (1988), 1896, 1913.
11. E. B. Bogomolny, *Zh. Eksp. Teor. Fiz.* **96** (1983), 487. [*Sov. Phys. JETP* **69** (1989), 275]
12. T. S. Monteiro and G. Wunner, *Phys. Rev. Lett.* **65** (1990), 1100.
13. P. A. Dando, T. S. Monteiro, D. Delande, and K. T. Taylor, *Phys. Rev. Lett.* **74** (1995), 1099.
14. B. Hüpper, J. Main, and G. Wunner, *Phys. Rev. A* **53** (1996), 744. B. Hüpper, J. Main, and G. Wunner, *Phys. Rev. Lett.* **74** (1995), 2650.
15. P. Kustaanheimo and E. Stiefel, *J. Ang. Math.* **218** (1965), 204.
16. M. V. Berry and K. E. Mount, *Rep. Prog. Phys.* **35** (1972).
17. V. P. Maslov and M. V. Fedoriuk, "Semi-classical Approximation in Quantum Mechanics," Reidel, Boston, 1981.
18. J. B. Delos, *Adv. Chem. Phys.* **65** (1986), 161.
19. J. Gao, J. B. Delos, and M. Baruch, *Phys. Rev. A* **46** (1992), 1449. J. Gao and J. B. Delos, *Phys. Rev. A* **46** (1992), 1455.
20. J. Hanssen, R. McCarroll, and P. Valiron, *J. Phys. B* **12** (1979), 899.
21. W. Schweizer, P. Faßbinder, and R. Gonzalez, *J. Phys. B*, in press.
22. J. Main and G. Wunner, *Phys. Rev. A* **55** (1997), 1743.